Geo-Marine Letters (2018) 38:195–209
https://doi.org/10.1007/s00367-018-0533-y

ORIGINAL

Large bedrock slope failures in a British Columbia, Canada fjord: first documented submarine sackungen

Kim W. Conway[1] · J. Vaughn Barrie[1]

Received: 1 December 2017 / Accepted: 17 January 2018 / Published online: 27 January 2018

Abstract

Very large (>60×10^6 m^3) sackungen or deep-seated gravitational slope deformations occur below sea level along a steep fjord wall in central Douglas Channel, British Columbia. The massive bedrock blocks were mobile between 13 and 11.5 thousand radiocarbon years BP (15,800 and 13,400 BP) immediately following deglaciation. Deformation of fjord sediments is apparent in sedimentary units overlying and adjacent to the blocks. Faults bound the edges of each block, cutting the glacial section but not the Holocene sediments. Retrogressive slides, small inset landslides as well as incipient and older slides are found on and around the large failure blocks. Lineations, fractures and faults parallel the coastline of Douglas Channel along the shoreline of the study area. Topographic data onshore indicate that faults and joints demarcate discrete rhomboid-shaped blocks which controlled the form, size and location of the sackungen. The described submarine sackungen share characteristic geomorphic features with many montane occurrences, such as uphill-facing scarps, foliated bedrock composition, largely vertical dislocation and a deglacial timing of development.

Introduction

The German term "Sackung" (plural "Sackungen") signifies a type of terrain sagging which commonly (but not exclusively) occurs in mountainous terrains (Helm 1932; Hutchinson 1988) where it often forms a diagnostic landform including uphill-facing scarps, elongate double-crested ridges and tension cracks (Pánek et al. 2015). These features are found in alpine areas globally, including California (McCalpin and Hart 2002), Italy (Ambrosi and Crosta 2005), Alaska (Li et al. 2012) and Canada (Schwab and Kirk 2002). Montane sackungen are normally linear deformations located along ridge crests and commonly occur in tectonically active areas (Agliardi et al. 2001; Sanchez et al. 2010) but are not a form of slide or creep as intimated by Zischinsky (1966; cf. also Poisel and Preh 2004, 2008). An important distinction between sackungen and landslides is the lack of significant lateral spreading in the former (Poisel and Preh 2004), though a bulge at the base of sackungen is frequently present. Sackung is not synonymous with deep seated gravitational slope deformation (DSGSD) but is considered to be a particular type of DSGSD (Soldati 2013). Sackungen are frequently associated with deglaciation of steep alpine landscapes (Hutchinson 1988). Some authors, however, reject the requirement for glaciation as a precursor to sackung formation (e.g. Pánek et al. 2015) and point to a lack of evidence for close timing of sackung formation and deglaciation. Others attribute the genesis of these features to a combination of climatic and tectonic processes (e.g. Gutiérrez et al. 2005). Foliated metamorphic rocks are key lithologies in the development of sackungen in the European Alps (Crosta et al. 2013) and they may also occur in a variety of other lithologies including soils and sedimentary rocks. Sackungen have to date not been identified in submarine environments as these features are typically associated with mountain range and ridge top settings, not valley floors. Accurate dating of the timing of initiation and activity of sackungen has been problematic at many sites.

While sackungen are normally slow, predominately vertical deformations, they have in some cases been shown to be a geological hazard stemming from sudden block sagging with devastating effects (Forcella 1984; Brückl 2001; Hewitt et al. 2008; Bianchi Fasani et al. 2014). In British Columbia (BC), Canada, sackungen have been reported at several locations on land (e.g. Thompson et al. 1997) and would have been prone to tsunami generation if occurring below the sea surface.

✉ Kim W. Conway
kconway@nrcan.gc.ca

[1] Geological Survey of Canada, Natural Resources Canada, 9860 West Saanich Road, Sidney, BC V8L 4B2, Canada

Thus, some of the largest tsunamis ever recorded have occurred in fjords as a result of slope failures (Bornhold and Thomson 2012). For example, a 524 m tsunami wave developed from a landslide in Lituya Bay in SE Alaska in 1958 (Weiss et al. 2009). The potential for large rock slides and sackungen to trigger tsunamis in coastal BC is therefore of concern as large events causing significant casualties have marked the past in this region (Bornhold et al. 2007). The British Columbia coast is earmarked by steep slopes, seasonal extremes of soil moisture, macrotidal conditions, and the highest seismicity in Canada, all of which increase the potential for slope failures in the form of slides and sackungen. In coastal environments, both submarine and subaerial slope failures may be initiated. Because such events generally take place in relatively shallow and confined waterways, they present a serious hazard for tsunami wave generation (Mosher 2009; Bornhold and Thomson 2012).

The Kitimat Arm and Douglas Channel fjord system is under consideration for the development of extensive shoreline installations and infrastructure for a variety of industrial projects mainly related to hydrocarbon port facilities. The proximity of large submarine landslides to the proposed infrastructure development has spurred research into the natural hazards associated with large slide masses and other submarine landslides in the region (Conway et al. 2012; Conway and Barrie 2015). The largest bedrock failures in Douglas Channel were described as possible submarine sackungen by Conway and Barrie (2015) and Shaw et al. (2017), and a late glacial timing was proposed for emplacement.

The purpose of this paper is to document the processes governing the development of these first identified submarine sackungen. It presents a detailed chronology for emplacement of these very large deformations, and provides information pertaining to the degree and nature of any potential geohazard which they may represent.

Regional setting

The coastline of British Columbia is dominated by steep coastal mountains and deep fjords which indent the coastline by up to 170 km. The Cordilleran hinterland of the mainland fjords is predominantly composed of plutonic bedrock (Wheeler et al. 1991). Douglas Channel, in particular, is a steep-sided fjord with depths up to 460 m (Macdonald et al. 1983). The northern portion of the BC coastal region was subject to extensive glaciation in the last glacial maximum (LGM), with ice thicknesses up to 2 km originating from inland ice depocentres (Clague 1984). Ice streams filled fjords locally to at least 1,000 m during the LGM and occupied the fjords from 25–16 ka BP. A discrete ice lobe extended beyond the mouth of Douglas Channel until about 13,000 years ago (Clague 1984). Sea levels were high due to isostatic depression of the region, leaving glaciomarine sediment at or above 200 m elevation between 10 and 13 ka BP.

Bedrock geology of the Douglas Channel/Kitimat Arm region of the Canadian Cordillera was studied by Roddick (1970). The geomorphology and orientation of Douglas Channel are thought to have been fault controlled (Duffell and Souther 1964; Roddick 1970; Holland 1976). The late Quaternary of the Kitimat region has been earmarked by glaciation and rapid sea-level change (Bornhold 1983; Clague 1985). During the LGM the fjord system was filled with ice. As ice margins retreated, thick sequences of mud, sand and deltaic gravels infilled basins in coastal settings as relative sea level fell. The present-day seafloor of Douglas Channel is underlain by up to 800 m of unconsolidated sediment (Bornhold 1983). Holocene sediments are up to 90 m thick in the deeper basin areas of Douglas Channel (Shaw et al. 2017) and overlie several hundred metres of glacial sediments including till (Bornhold 1983). The Hawkesbury Island marine study area (Fig. 1) was fully covered by ice until 12 ka BP.

The oceanography of the Douglas Channel fjord system is the subject of ongoing study (Johannessen et al. 2015) and was last reviewed by Macdonald et al. (1983). The fjord has a well-developed estuarine circulation and bottom water exchange occurs on an annual timescale through channels to the continental shelf. Particles accumulate in the fjord from rivers and streams entering both at the head and along sidewalls of the fjord system. Sediment accumulation has been uneven due to variable tidal currents at the seafloor (Shaw et al. 2017) and Holocene deposition varies from 0 to 90 m in thickness, and in some areas the glaciomarine section is exposed and eroding. Regionally, landslides were mapped in Douglas Channel and Kitimat Arm and other coastal areas by Conway et al. (2013), and large submarine failures and tsunami potential of failures within Douglas Channel were documented (Conway et al. 2012; Thomson et al. 2012).

Within the study area, extensive north–south oriented lineaments show evidence for possible faulting (Conway et al. 2012). However, there has been only very limited seismicity, with a total of eleven magnitude <3.0 earthquakes in the last 25 years in the proximity of the study area (Geological Survey of Canada (GSC), unpublished data). Understanding the process and timing of submarine slope failure is critical to gauging the hazard represented by slope instability. The tsunamigenic potential of creep or slowly moving failures is much reduced compared to any rapidly occurring event. In addition, it is understood that slope instability and failure was much more common during the immediate post-glacial time period than in more recent (Holocene) times (St. Onge et al. 2004). However, the presence of submarine failure deposits in the present-day landscape is not necessarily an indication of an ongoing hazard (Conway et al. 2013).

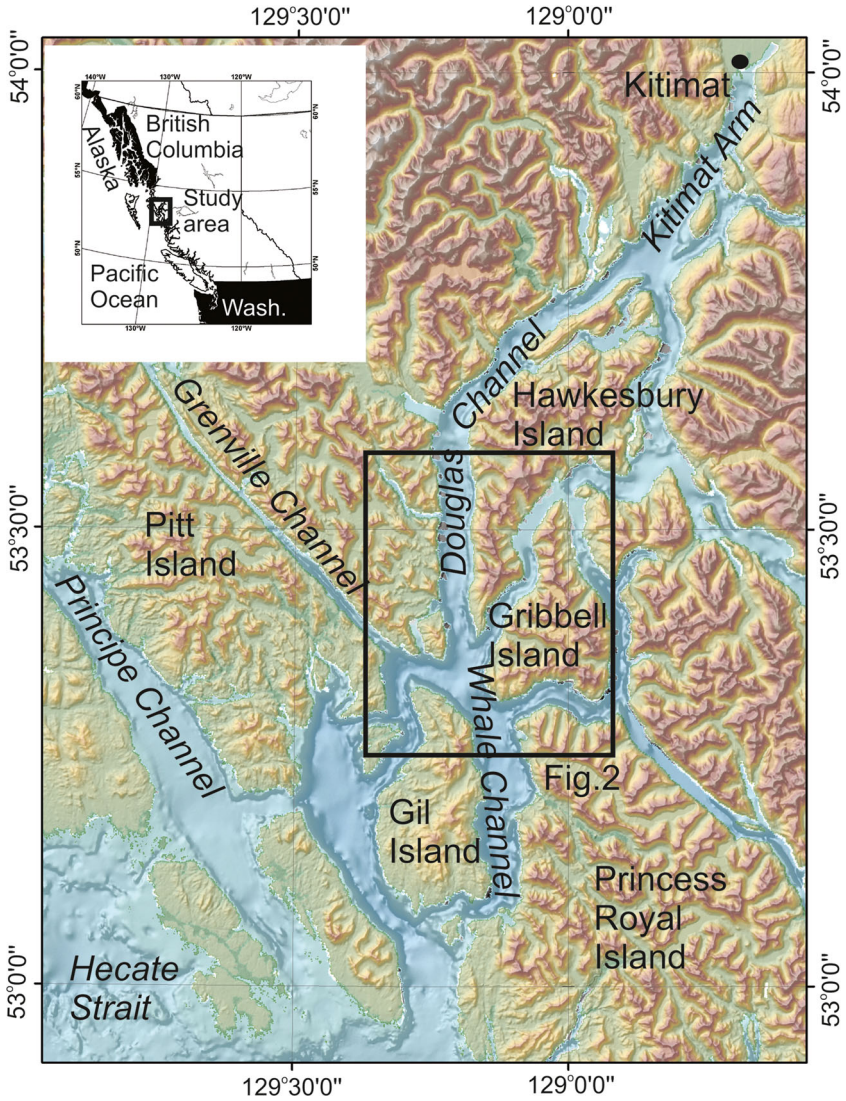

Fig. 1 Location of the Douglas Channel/Kitimat Arm study area with regional topography and bathymetry. Extracted from Conway and Barrie (2015)

Materials and methods

Marine geoscience investigations have been undertaken to study previously defined slope failures in Douglas Channel (Conway et al. 2012; Conway and Barrie 2015) in order to assess the nature, age and origin of the largest failure features and shallow faulting of the seafloor. Multibeam data were collected in Kitimat Arm and Douglas Channel by the Canadian Coast Guard Ship CCGS *Vector* between 2007 and 2010 using a hull-mounted Kongsberg-Simrad EM2002 multibeam echo-sounder system before 2009, and a Kongsberg-Simrad EM 710 system operating at 70–100 kHz system mounted in a gondola after 2009 in water depths greater than 50 m. Inshore areas of >5 m depth were surveyed by the CCG Launch *Otter Bay* using a EM 3002 multibeam system. Data were gathered using the Kongsberg SIS system and processed using the CUBE extension of CARIS-HIPS software. Data were then exported as 5-m resolution grids with confidence intervals of 0.1% of water depth vertically and 2 m laterally. Lateral errors arise from navigational limitations. The grids were then imported into ESRI ArcInfo© GIS software to allow visualization. Perspective, three-dimensional views of samples of the multibeam datasets were created using Fledermaus© software.

Marine geophysical surveys were completed on CCGS *Vector* cruise 2013007PGC in November 2013 and from CCGS *John P. Tully* in October 2014. Roughly 220 line km of high-resolution seismic sparker data were collected using a 400 joule Huntec deep-tow seismic (DTS) system during the 2013 survey (Fig. 2). In addition, 500 line km of chirp profile data were collected during both cruises, operating at a nominal frequency of 3.5 kHz. Kingdom Suite software allowed processing and analysis of sparker and chirp sub-bottom data.

A Benthos piston coring system with a 1,000 kg head weight allowed cores to 8 m length to be collected (Fig. 2). A digital camera (GSC-A 4000) was employed in 2014 and a

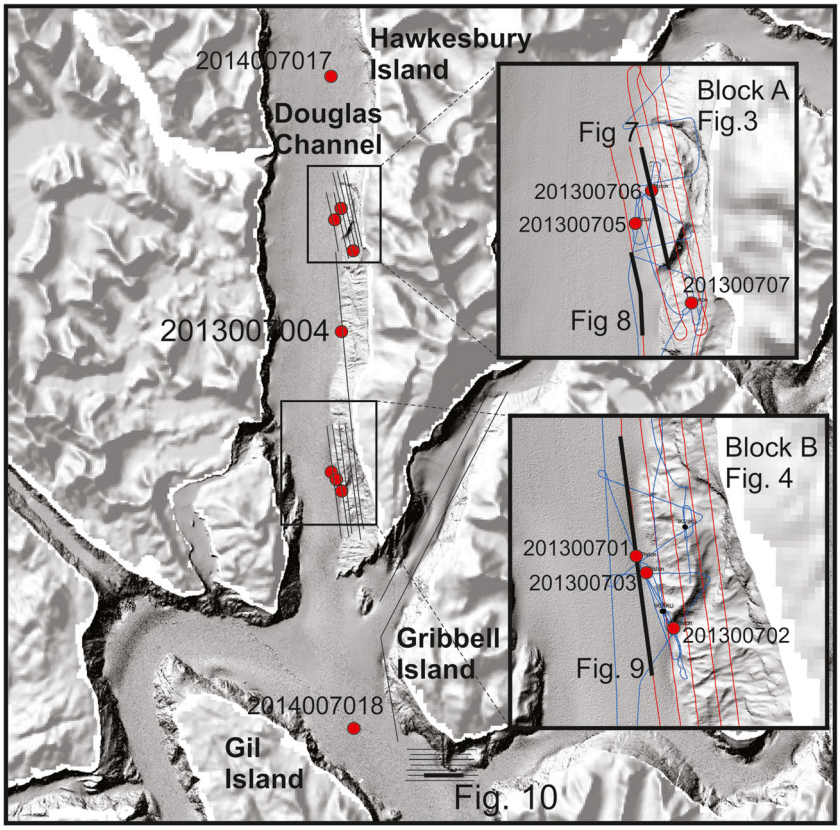

Fig. 2 Douglas Channel study area. Insets location of Cruise 2013007 cores and figures relative to blocks A and B. Extracted from Conway and Barrie (2015)

large volume (0.5 m^3) grab sampler was used during the 2013 cruise. The remote operated vehicle ROPOS (Dive R1877) was deployed in September 2015 to examine the head scarp of a large slope failure (cf. block A below). Light detection and ranging (LiDAR) data were collected onshore, adjacent to the marine study area, between April and June 2015 using a Riegl VQ-580 LiDAR system.

GeoTek© multi-sensor core logger (mscl) systems served to analyse the cores for physical properties including gamma-ray density, magnetic susceptibility and high-resolution imaging. Note that these data are not reported in the present study. Cores were visually logged after splitting. Sediment textures were described conforming to the Wentworth scale (Wentworth 1923) from grain size datasets (GSC unpublished data) which were calculated by the method of moments with analysis of mud fractions by Micromeritics Sedigraph©, sand by settling column, and gravel by sieve. Cores were rendered as graphic logs after the method of Boyles et al. (1986).

Accelerator mass spectroscopy radiocarbon dating of selected core samples was performed at Beta Analytic Inc. Ages are presented and discussed in conventional radiocarbon years before present (BP). A reservoir correction of 800 years was applied to shell dates (410 global reservoir and a 390 year local marine reservoir Delta-R correction). Conversion of radiocarbon years to calendar years was accomplished using the algorithm of Fairbanks et al. (2005).

Results

Multibeam bathymetric data illuminate two areas of massive slope failure along the south-eastern margin of Douglas Channel (Fig. 1). Seabed sample locations, geophysical survey transects and figure locations are shown in Fig. 2. The fjord wall appears to have failed where two scallop-shaped hollows located along the edge of the fjord wall are closely associated with detached blocks apparent on the fjord floor. The northern failure (block A) appears to originate from sea level to 100 m depth along the shoreline (Fig. 3) whereas, to the south, block B has a source from 75 to 100 m depth (Fig. 4). The bedrock composition of the blocks is inferred to be derived directly from the Hawkesbury Island coastal lithology which, according to the mapping by Roddick (1970), consists of a diorite (igneous) rock type at block A and a gneissic-diorite migmatite at block B. ROV observations at block A were able confirm this lithology, and also discriminate well-developed joints and fractures on the vertical wall of the head scarp.

The failure masses rest on the fjord floor where a drape of mud covers the surface morphology of the base of the block at approximately 350 m water depth at block A and 400 m at block B. The margins of the failures are mantled with thick recent sediments (Figs. 3 and 4) which also infill the fjord. The seafloor morphology suggests that a portion of each failed block extends for some distance onto the fjord floor, where

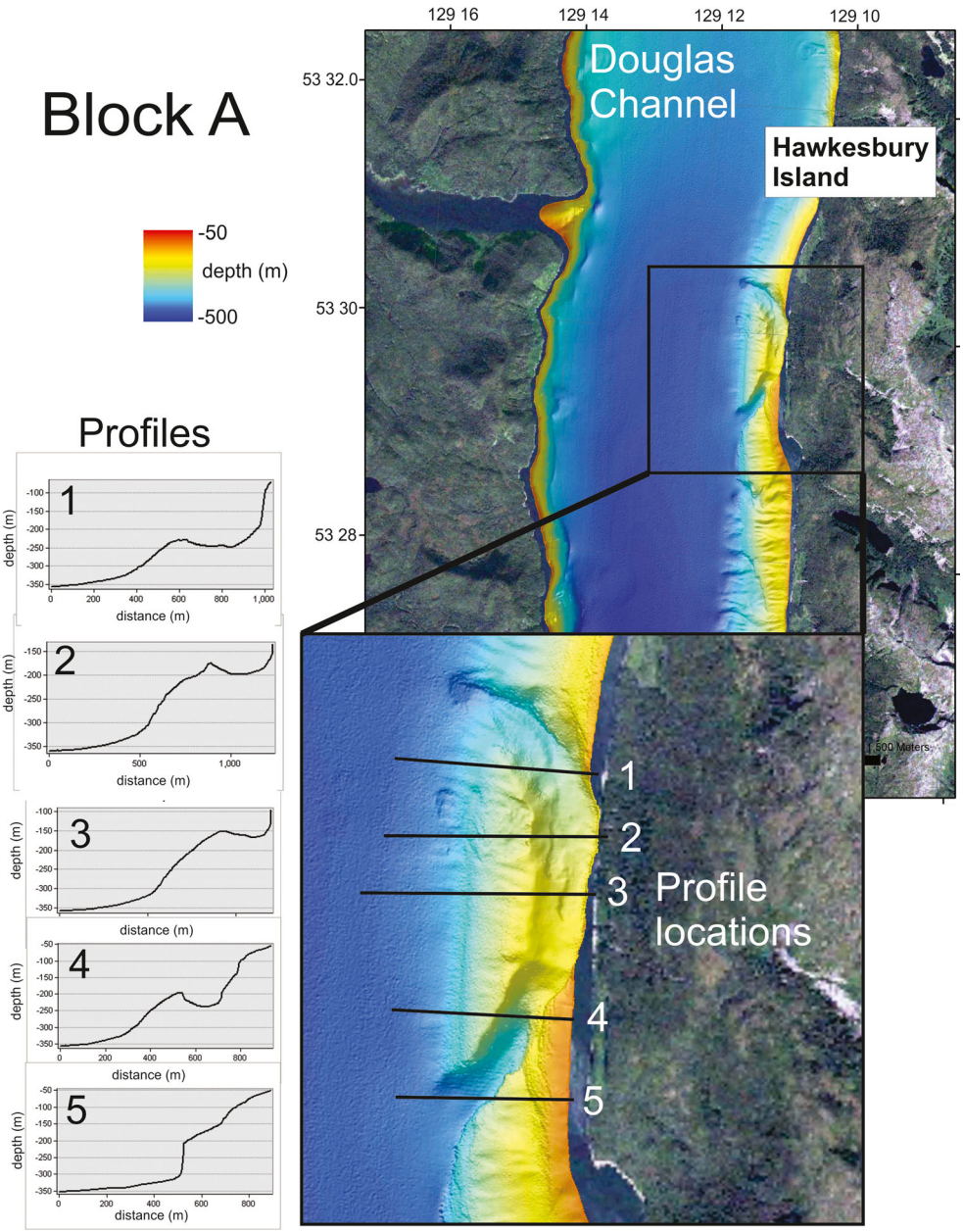

Fig. 3 Detailed multibeam imagery of block A. Bathymetric profiles extracted from multibeam bathymetry data are shown with locations at right. See Fig. 2 for location. Profiles show general shape of block detachment from Hawkesbury Island. Profile 5 shows 100 m scarp where block was removed. Extracted from Conway et al. (2012)

they have been subsequently buried by sedimentation (Figs. 3 and 4). Bathymetric profiles across the blocks (Figs. 3 and 4) indicate that they have moved into place after detachment and that this motion has moved block A downslope by up to 350 m and block B by up to 400 m. The profiles also show that the evacuated head scarps of both blocks are nearly vertical. Relative block movements are not the same along the north–south oriented centre axes of the blocks relative to the source of the failure, and both blocks indicate more downslope movement on the southern side of the mass than on the northern side. The volumes of the failed blocks are calculated to be 62×10^6 m^3 for block A and 70×10^6 m^3 for block B (Thomson et al. 2012).

Perspective views of block A looking northwards up the channel (Fig. 5) show that the block is set within a zone of general slope instability where relatively small slides are superimposed on the large bedrock masses. Small slides occur both on the back, landward-facing slope of block A and also at the crest of the same block, facing seawards. An adjacent, somewhat muted scarp appears to define a potential incipient failure immediately south of block A (Fig. 5). This area is bracketed by block A to the north and retrogressive, small slides to the south at the base of the fjord slope. In addition, an older failure scarp is apparent further to the south (Fig. 5).

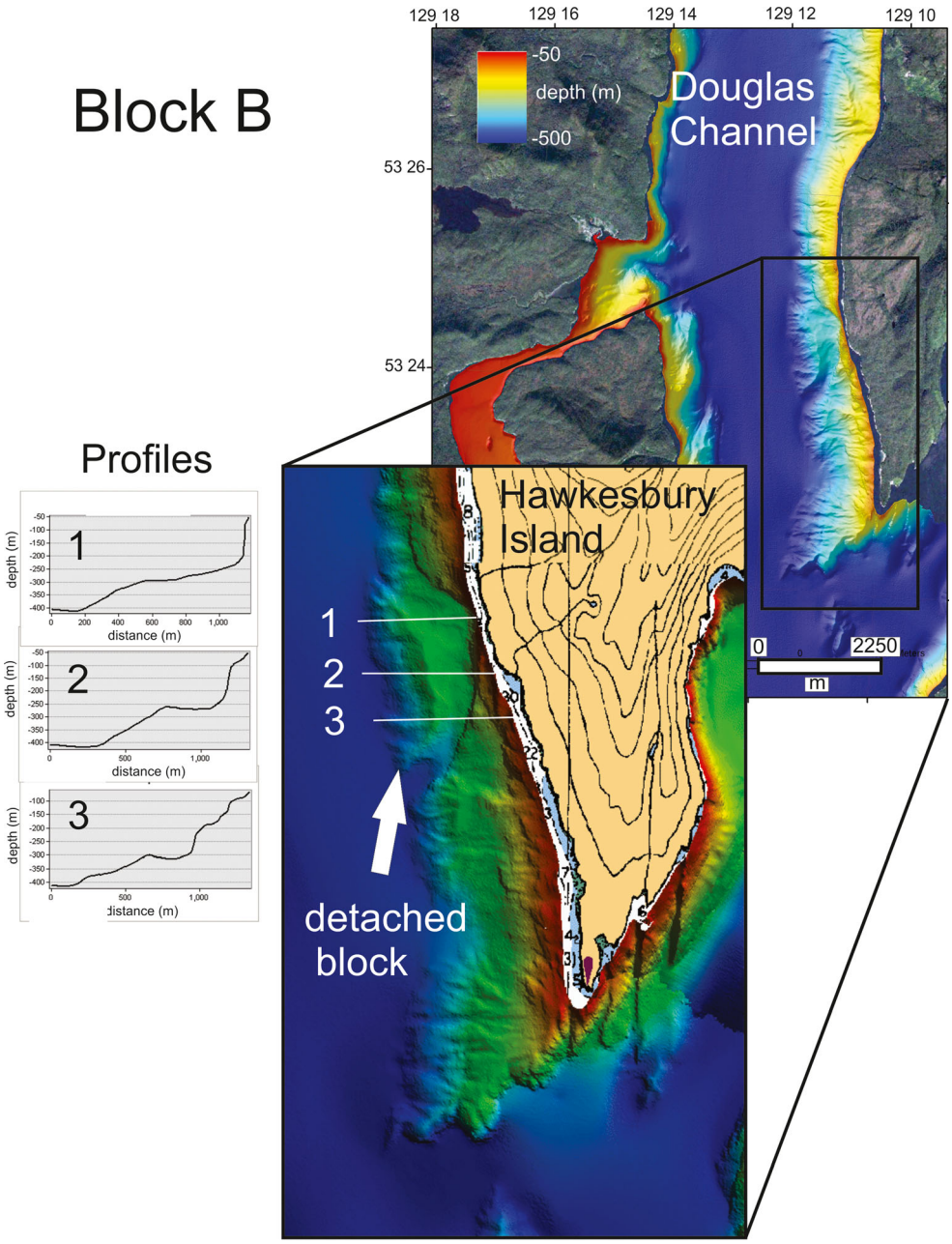

Fig. 4 Detailed multibeam imagery of block B showing detachment area. Bathymetric profiles extracted from multibeam bathymetry data are shown with locations at right. See Fig. 2 for location. Note pronounced north-trending submarine fractures at the south end of Hawkesbury Island. Extracted from Conway et al. (2012)

Sedimentary units and geochronology

Coring results from Douglas Channel describe a sequence of three widespread surficial units (Fig. 6). A lower unit (here designated unit 1) is a laminated to massive grey clay with sparse sand and gravel clasts. The unit, up to 6 m thick (2013007PGC cores), contains sand grains and gravel clasts of various lithologies which are matrix supported in the clay. Unit 1, dated to 10,110±30 to 10,950±40 radiocarbon years before present (C14yBP; Fig. 6, Table 1), also yielded one young age of 4,630±30. An interbedded silty clay to variably coloured well-sorted clay (unit 2) overlying the gravel clay unit yielded ages from 10,470 to 10,200 C14yBP. The clay beds vary from 10 to 40 cm in thickness and are burrowed in some intervals. The clays, coloured blue-grey to blue-green, are a markedly different colour than the bracketing grey to dark grey mud unit.

The topmost unit (unit 3) is an olive, soft and massive bioturbated silt which is up to 5.5 m thick in the cores (Fig. 6). The unit is completely bioturbated and is entirely massive in character. Cores sampled variable unit 3 sediment thicknesses but nowhere did the unit contain bedding or laminations. Ages in unit 3 ranged from 4,250±30 C14yBP at 144 cm depth in core 2014007018 to 10,230±30 C14yBP at 429 cm depth in core 2013007003 (Table 1). The uppermost unit has been accumulating at a variable rate in Douglas

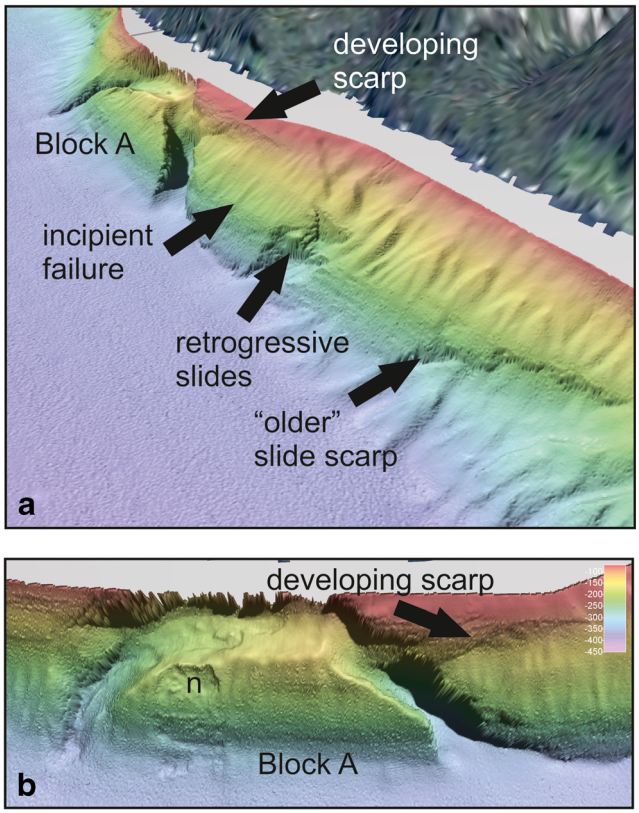

Fig. 5 Perspective views of block A and surrounding area using Fledermaus software. **a** Oblique view looking north shows several instability features adjacent to block A, including an older slide scarp and a possible incipient slide bracketed by block A and smaller retrogressive slides. **b** Oblique view looking east towards block A shows several small slides (at *n*) on the top and the back slope of the main slide, and a close-up of what may be a developing slide or sackung scarp. Extracted from Conway et al. (2012)

Channel and the range of radiocarbon ages indicates sedimentation throughout most of the Holocene.

At two core sites (2013007006 and 2013007007) adjacent to blocks A and B (Fig. 2), no unit 3 sediments have accumulated and unit 1 (glaciomarine gravelly and laminated grey clay) formed the entire core. Two core sites (2014007017 and 2014007018), distal from the blocks, were sampled to allow study of regional sedimentation (Fig. 2). These recovered a similar lithologic section and provided similar radiocarbon ages. Estimated sedimentation rates were 0.7 and 0.9 mm per year at these sites respectively during the deposition of unit 3. No stratified sections indicative of events were observed in the cores. Multi-sensor core logger data indicate that unit 3 is completely unstratified, resulting from uninterrupted, slow and well-bioturbated sedimentation.

Sedimentary sequence

The lowermost unit (unit 1) is related to the latest stages of deglaciation of the study area. Isolated gravel clasts and coarse sand grains were deposited as ice-rafted debris (IRD). Silt and very fine sand laminae likely represent glaciomarine pulses and underflow deposition of sediment from turbid glacial melt water. The radiocarbon ages obtained in this unit correspond with a late deglacial time of deposition from 11–10.5 ka BP.

The clay unit (unit 2) which overlies unit 1 is a stratified, anomalous deposit evidenced by the variable colour hues in the well-sorted beds. Radiocarbon ages of 10.5 to about 10.2 ka BP, blue-grey sediment colour, and slightly bioturbated nature of the unit indicate that it records the final phase of deglaciation, before the onset of a truly Holocene climatic and oceanographic environment.

The topmost unit in the sequence (unit 3) is of Holocene age and is completely bioturbated, massive and olive in colour. The recent sedimentation rate is variable throughout Douglas Channel due to variability in the velocity of seabed tidal currents and to geostrophic effects which modify currents and influence deposition in the fjord. At some locations Holocene sediments are up to 90 m thick, while in other areas which are subject to seafloor scour and even erosion, no sediment has accumulated. Sedimentation rates in unit 3 were found to be less than 1 mm per year at all core sites. Recent sedimentation was absent on blocks A and B and these areas are non-depositional. The massive Holocene sedimentary sequence is nowhere interrupted by graded sand beds or silty laminae.

Glaciomarine sequence deformed by blocks A and B

In the periphery of block A deformation, as imaged in sub-bottom profile data, suggests impact on a deforming front of the well-stratified glacial marine sediments of unit 1. Deformed and gently folded or buckled glaciomarine sediments are observed overlying and adjacent to the seaward edge of the blocks. The folds appear as muted anticlines of 100 to 300 m width with indications of brittle deformation at the boundaries of the weakly developed folds which may be up to 50 m thick (Fig. 7). The folded, deformed reflectors do not appear as one deformed section but as several intervals forming a deformed complex overlying the bedrock failure. Localized folds are, in some cases, capped by debris flows. In sub-bottom profile data at the boundary of block A, brittle deformation of the section may be clearly seen (Fig. 8).

At block B the deformed interface is draped, and the uppermost sequences have been folded and deformed successively (Fig. 9). This implies that the blocks were not emplaced in an instantaneous event during a single dislocation. Brittle deformation at block B is seen at bounding faults and this is capped by sediments which show subsequent draping and further folding followed by debris flow deposition (Fig. 9). The glacial sequence is draped by undeformed horizons which include the uppermost (latest) glacial sediments.

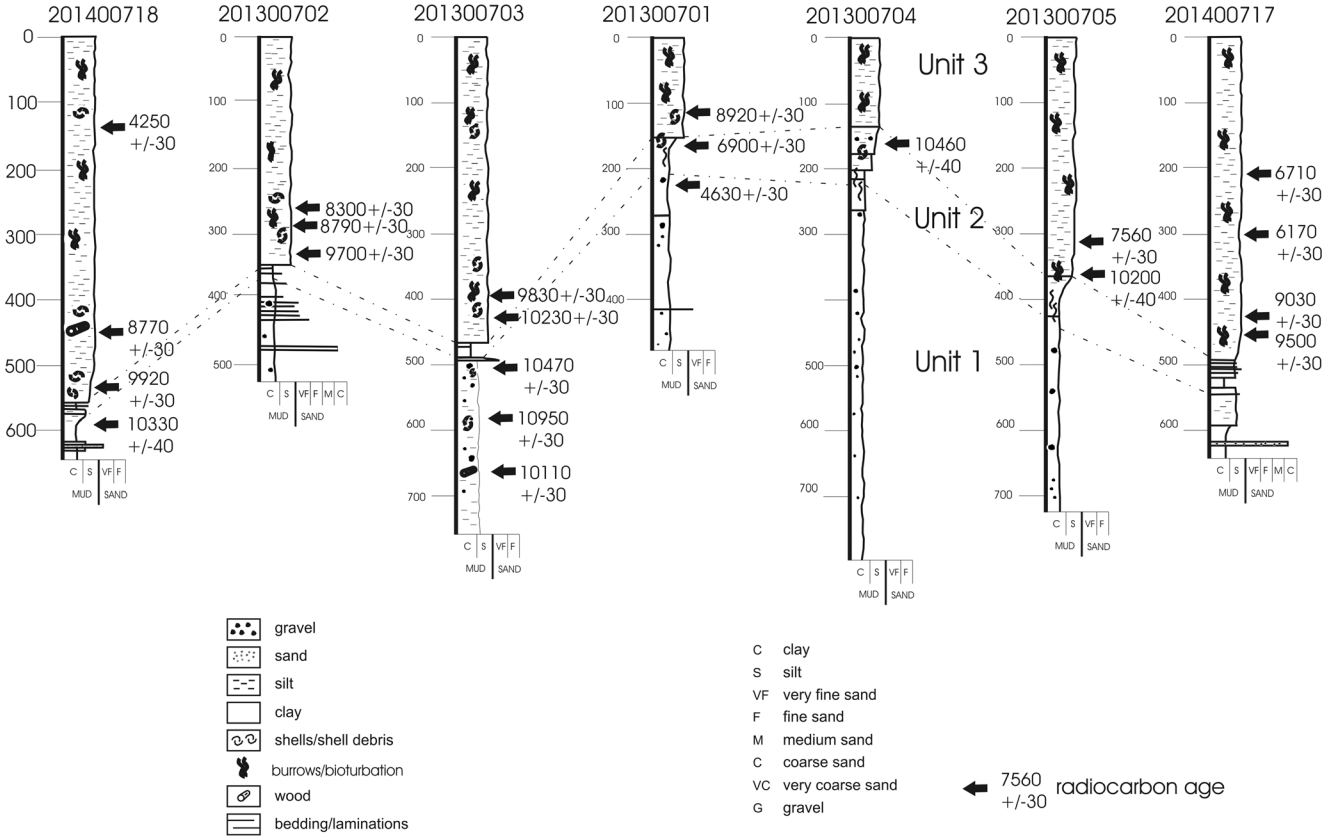

Fig. 6 Douglas Channel piston core lithology, ages and correlation. See Fig. 2 for locations. Extracted from Conway and Barrie (2015)

Identification of late quaternary faults

Evidence of active faulting is seen at three locations in the sub-bottom profile data. Reflector offsets are apparent in the glacial section at the southern edge of the flank of block A (Fig. 8). Further to the south, block B is bounded on both sides by fault offsets which penetrate from the bedrock through the overlying glacial sediments (Fig. 9) with reflectors offset up to 60 m. The sediments have been dislocated by the block-bounding faults in a brittle fashion. The data do not resolve the initiation of the faults, presumably located deep in the bedrock.

Near the southern end of Gribbell Island (see Figs. 1 and 2 for location), seismic profiles indicate that the glaciomarine section is faulted beneath the seafloor (Fig. 10). The deformation coincides with the strike of a prominent lineament which sections Gribbell Island. The deformation of the geologic unit is post-depositional and not an on-lapping or draping relationship of reflectors to an adjacent or buried surface. The fault does not entirely cut the glacial section nor is the Holocene sequence penetrated (Fig. 10). The top of the faulted section has been eroded and this sequence has been buried by subsequent glacial and Holocene deposition which remains undeformed. The faulted section displays little vertical offset.

LiDAR data

The Hawkesbury Island shoreline is the source of blocks A and B found along the eastern edge of Douglas Channel. Regionally extensive north–south lineaments can be seen in bathymetric and topographic data in this area. LiDAR data (Fig. 11) show the gross nature of the shoreline structural elements in the vicinity of block A where joints and faults appear to define lozenge-shaped bedrock slabs which demarcate potential detachments from the shoreline above the block. During a ROV transect along the back scarp of block A, well-developed foliation and fracture planes were noted in the bedrock wall, as well as density and salinity anomalies indicating freshwater flow through horizons in the bedrock.

Discussion

The bedrock walls of Douglas Channel would have been greatly smoothed, and the fjord floor excavated during massive ice movement through the entire fjord system between 25 and 14 ka BP (Clague 1985). If the blocks had been emplaced before the last glaciation, then the head scarps would have

Table 1 Radiocarbon ages of samples from Douglas Channel piston cores. A local marine reservoir correction (Delta-R = –390 years) and global reservoir correction (–410 years) were applied to shell dates for a total radiocarbon marine reservoir correction of –800 years. Extracted from Conway and Barrie (2015)

Core number	Depth in core (cm)	Beta analytic lab. number	Material	Conventional radiocarbon age (years BP)	Calendar age[a]
2013007001	113	384642	Shell	8,920±30	10,096±87
2013007001	156	384643	Shell	6,900±30	7,714±33
2013007001	226	384644	Wood	4,630±30	5,362±55
2013007002	266	384645	Shell	8,300±30	9,315±58
2013007002	282	384646	Shell	8,790±30	9,798±81
2013007002	340	384647	Shell	9,700±30	11,160±34
2013007003	394	384648	Shell	9,830±30	11,229±15
2013007003	429	384649	Shell	10,230±30	11,977±62
2013007003	502	384650	Shell	10,470±30	12,415±60
2013007003	581	384651	Shell	10,950±40	12,834±46
2013007003	667	384652	Wood	10,110±30	11,729±77
2013007004	160	384653	Shell	10,460±40	12,393±81
2013007005	311	384654	Shell	7,560±30	8,377±16
2013007005	363	384655	Shell	10,200±30	11,922±73
2014007017	208	405125	Shell	6,710±30	7,576±19
2014007017	301	405126	Wood	6,170±30	7,065±60
2014007017	432	407367	Shell	9,030±30	10,209±14
2014007017	453	405127	Shell	9,500±30	10,755±80
2014007018	144	405128	Wood	4,250±30	4,832±19
2014007018	450	405129	Wood	8,770±30	9,753±72
2014007018	536	405130	Shell	9,920±30	11,292±37
2014007018	592	407368	Shell	10,330±40	12,124±78

[a] Fairbanks et al. (2005) calibration algorithm

been greatly modified, and the rock blocks eroded and rounded and traces of the block motion largely removed during long-term glacial ice movement through the fjord. The dislocation of blocks A and B must have occurred during regional deglaciation and after ice had locally receded from the Douglas Channel failure sites. Examination of multibeam data from all other BC fjords surveyed to date does not reveal any similar submarine failures of this scale and form (Conway et al. 2013.). The processes and timing of ice advance and deglaciation would have been quite similar in adjacent BC fjords, suggesting that local variation in rock properties and structural relationships play a role in the development of the failure blocks in Douglas Channel.

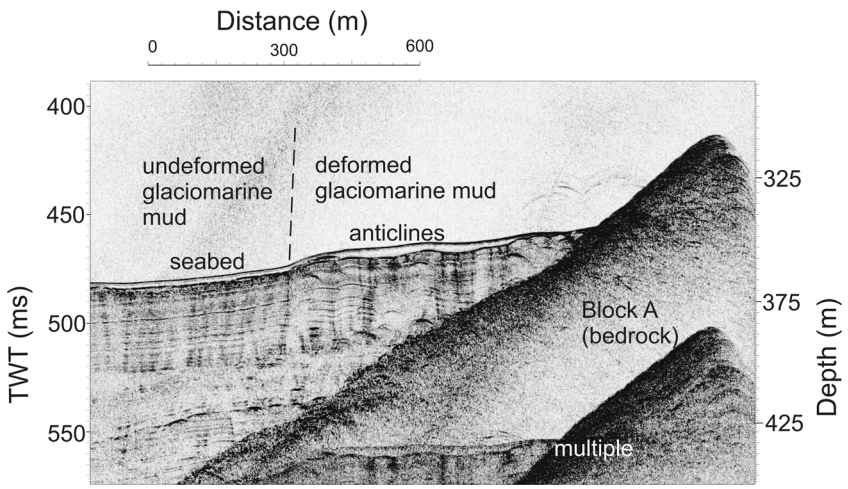

Fig. 7 Huntec DTS profile showing stratified and deformed glaciomarine sequence at block A. See Fig. 2 for location. Extracted from Conway and Barrie (2015)

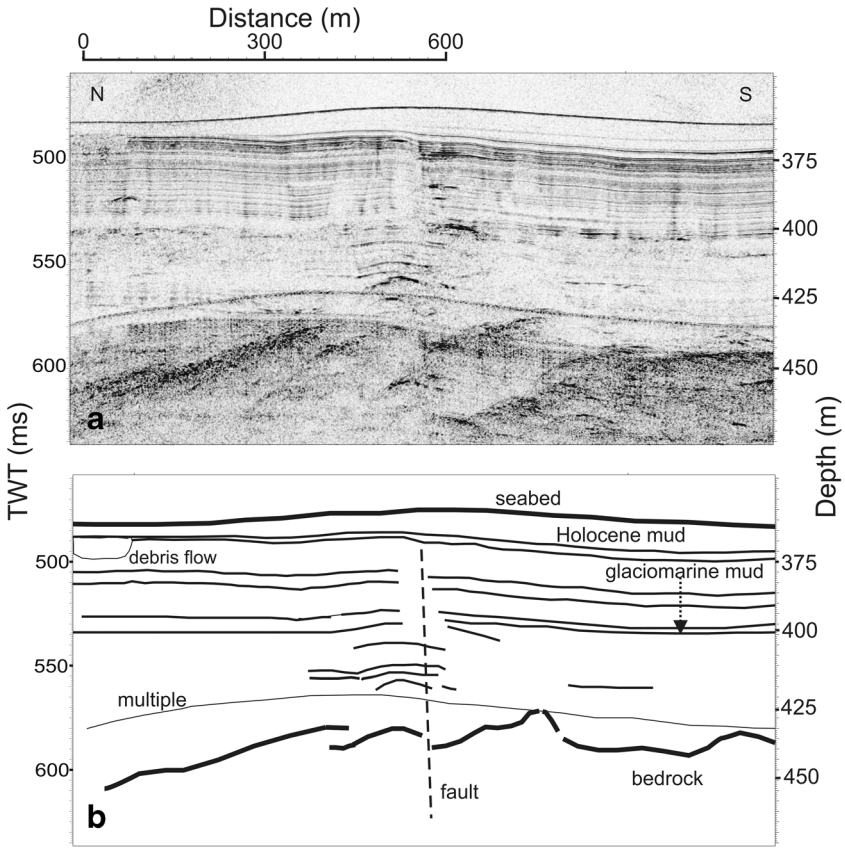

Figure 8

Fig. 8 High-resolution sub-bottom profile adjacent to block A. **a** Huntec DTS geophysical profile. **b** Interpreted section showing faulted sediments. See Fig. 2 for location. Extracted from Conway and Barrie (2015)

Slope instability—blocks A and B

Late glacial sediments are seen to be deformed and folded in high-resolution seismic data in proximity to blocks A and B while the Holocene section is not affected. The bounding faults that demark the edges of blocks A and B do not penetrate the upper part of the glaciomarine sequence. The undeformed upper portion of this glacial sequence would date from the latest phase of deglaciation when ice had receded from the immediate area and up Douglas Channel towards Kitimat Arm, where an ice front was present by roughly 11.5 ka BP (Bornhold 1983). The timing of the active period of the motion of the blocks is thus estimated at between 13 and 11.5 thousand radiocarbon years BP (15,800 and 13,400 cal years BP).

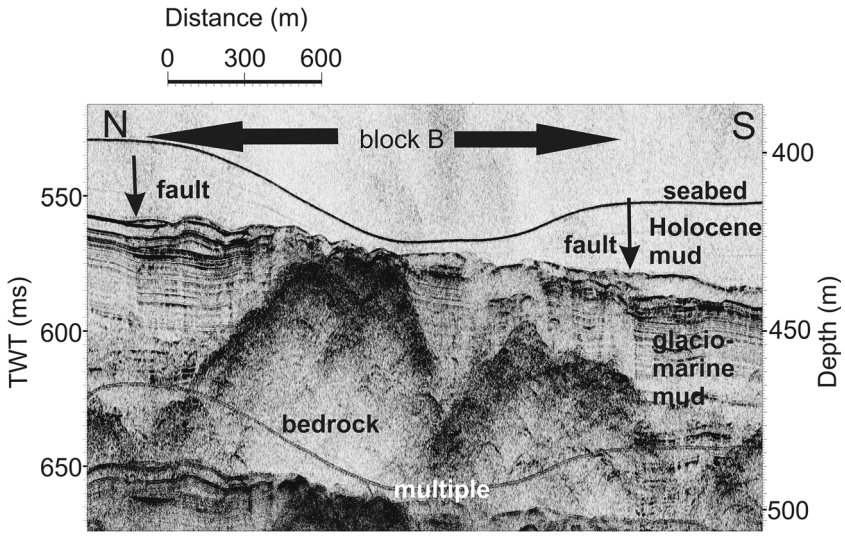

Fig. 9 High-resolution sub-bottom profile adjacent to block B showing faulted strata below the Holocene and late glacial section. See Fig. 2 for location. Extracted from Conway and Barrie (2015)

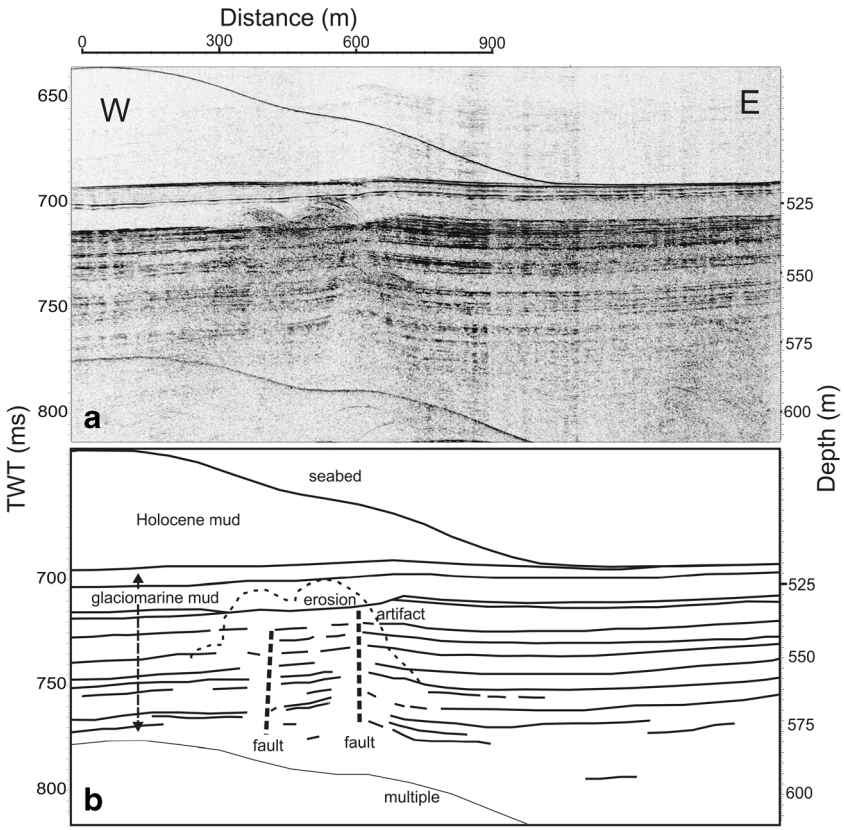

Fig. 10 High-resolution sub-bottom profile south of Gribbell Island. **a** Huntec DTS geophysical profile. **b** Interpreted section showing faulted sediments. See Fig. 2 for location. Extracted from Conway and Barrie (2015)

Seismic data indicate that the deformation of the glacial sequence adjacent to and overlying blocks A and B was incremental and punctuated by intermittent loading or impact on the well-stratified section. Observations in the sub-bottom data of a series of low dip angle and relatively broad folds and buckled sequences in juxtaposition to brittle fault deformation at block edges are consistent with incremental as opposed to instantaneous disruption of the sequence. Were an instantaneous impact of the very large blocks A and B to collide with a well-bedded stratigraphic sequence, it would imply the

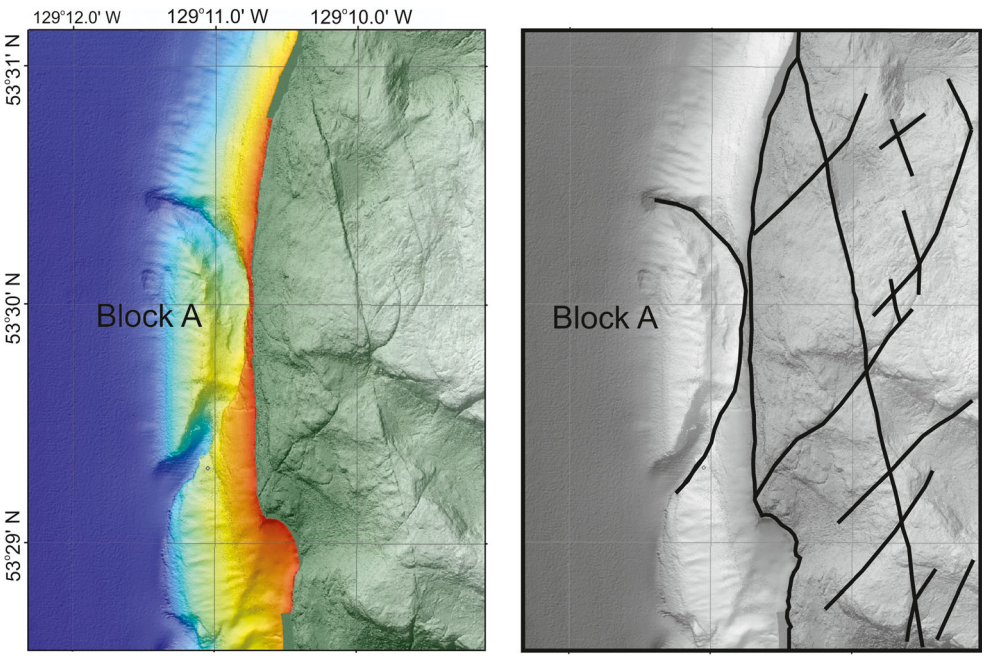

Fig. 11 Multibeam and LiDAR data collected near block A (left), and location of main faults, fractures and joints along the Hawkesbury Island shoreline (right)

creation of thrust features within the sedimentary section. Such thrust features are not observed in the sub-bottom data, and a gentle and discontinuous deformation style of low angle folds is seen with only minor small massive intervals noted. Such massive chaotic seismic units, indicative of debris flows, are largely restricted to the inshore areas of the blocks and are found to intercalate and cap both the folded as well as the undeformed glacial sections at some locations.

Sea levels during the time period of active movement (15,800 to 13,400 cal years BP) would have been changing rapidly with inundation of deglaciated landscapes as ice receded. Isostatic loading of the coastal mountains would have ensured that the crust remained depressed as ice receded and allowed inundation to occur, though the existence of a pronounced glacial forebulge to the west complicates this sea-level scenario somewhat (Hetherington et al. 2004). Sea levels were 200 m above present at Kitimat at 10 ka BP (Clague 1985). Blocks A and B formed in a setting which had been newly deglaciated, where sea levels were not stable and where fractures and faults would have been conduits for melt water and provided lubrication during block movement.

Small slides originating near the top and from the sides of block A were composed of gravelly grey glacial marine clay and these are post-glacial in age. These small translational slides may have been initiated from the motion of the block in late glacial time or alternately are due to subsequent, more recent Holocene slope instability. Some small slope failures at the edges of the blocks are also composed of glaciomarine sediments, and the chronology of these slides is uncertain as much of the area adjacent to the blocks is non-depositional. Evidence of regional landscape instability is reflected in cored sequences including unit 2, an anomalous clay deposit. The unit is similar in texture, stratigraphic position and colour to clays which record glacial lake outburst flood events in the BC shelf and fjords to the south (Conway et al. 2001; Blais-Stevens et al. 2003). Further study of cored intervals of unit 2 could confirm this interpretation. Thick deposits of regionally distributed clays have been attributed to such outburst floods in the Douglas Channel region (Shaw et al. 2017).

Recent faulting

Examples of fault offsets in glacial sediments are observed in the high-resolution profile data. Seismic data indicate about 10 m of vertical offset at one site adjacent to and offshore of the southern limit of block A (Fig. 8) and also at block B at both ends of the block (Fig. 9). Faulting has also affected glacial sediments at the southern end of Gribbell Island where strong surface lineations have also developed. The faulting at the margins of blocks A and B is related to block emplacement and accompanied the downward movement of the blocks. Deformation of the glacial section related to emplacement of the bedrock masses is apparent at both sites. The seismic data through to the base of the resolved interval indicate brittle deformation and offset reflectors on discrete planes. The trend of the faults, which are roughly at a 30 to 45° angle, suggests that they may be synthetic or normal faults related to a main system of north–south faults. The shallow submarine faults combined with the onshore fractures of the margins of Douglas Channel suggest that a distributed style of deformation may exist. Minimal vertical offset is seen on the Gribbell Island fault trace, which is unsurprising considering the fault is likely part of a strike slip pattern of local faulting. The identified fault trace aligns with a well-defined lineament which bisects Gribbell Island and extends offshore to the south, seen in multibeam datasets (Conway et al. 2012). This north–south trending fault was probably reactivated by the isostatic effects of ice loading. It is also possible that the modern stress regime is implicated in this faulting. Precision GPS monitoring in the region has defined broad north–south dextral shear (Mazzotti et al. 2003, 2011), which is opposite to the left-lateral strike slip motion inferred for the Douglas Channel area. While these motions are not mutually exclusive, the left-lateral motion along Douglas Channel must be accommodated by block rotation within the larger right-lateral shear, tectonic situation.

The structural control on major physiographic elements of the Douglas Channel/Kitimat Arm area has been inferred to be north–south trending (Duffell and Souther 1964; Bornhold 1983). The main structural alignment in the adjacent region to the west and north is associated with the well-described Grenville Channel fault system which trends NW–SE (Nelson et al. 2011). While no faults are indicated on geologic maps of the area (Roddick 1970), a series of foliation directions are indicated as being coast parallel in the area of the slides on Hawkesbury Island. Duffell and Souther (1964) and Roddick (1970) both suggest that faults offset the two sides of Douglas Channel and Kitimat Arm, both of which represent structurally controlled north–south physiographic landforms (Holland 1976). The sense of motion of the inferred faults was up and to the north on the eastern side relative to the western side of Douglas Channel (Roddick 1970).

Sackungen

Geological and geophysical data indicate that blocks A and B were emplaced in a punctuated fashion and not catastrophically. The deformation observed in the glaciomarine sediments peripheral to the blocks is consistent with a slow sagging impact as opposed to catastrophic dislocation from instantaneous failure. The cored sequences and radiocarbon chronology indicate that the blocks date from the deglaciation of Douglas Channel. The attributes of the blocks including massive size, thickness and shape, limited downslope and peripheral deformation and the uphill-facing scarps are all consistent

with the features having origins as sagging blocks, or sackungen sensu Helm (1932) and Hutchinson (1988).

Bedrock structural control of the shape and dimensions of blocks A and B is apparent in sub-bottom and topographic data. LiDAR data show the main trend of joints and faults above block A on Hawkesbury Island. It is inferred that this clear structural pattern has contributed to the generation of the sackungen in Douglas Channel. This is conceptually illustrated in Fig. 12. Observations of well-developed foliation planes in the bedrock wall of the scarp at block A, and water density anomalies at these layers indicate freshwater flow focussed along these horizons. Flow of this kind along planar discontinuities in the bedrock would have provided lubrication during movement of the bedrock masses.

Dating of sackungen movement rates on land is normally accomplished by boreholes collected in the back scarp of the deformed area which is typically infilled during its development. Typical rates of sackung movement measured on land are a few mm to a few cm per year (Forcella 1984; Hippolyte et al. 2012). In the case of the Douglas Channel, the back scarps are not infilled, so that this method of dating is not possible. The area is non-depositional due to high ambient seabed tidal currents keeping the displaced masses swept clear of recent sediments. Blocks A and B have downslope dislocations of 300–400 m. If these blocks are associated with sackung style deformation, then 300–400 m of movement would have been accommodated between about 13,000 and 11,500 radiocarbon years BP (15,800 and 13,400 BP) when ice receded from the outer Douglas Channel landwards to Kitimat Arm (Bornhold 1983), and before the latest glaciomarine sediments were deposited. This would give an estimated sackung development rate of about 13–17 cm per year. This more rapid rate of movement may be related to the submarine setting of these features, where presumably lubrication along bounding surface planes would be more complete.

Compared to blocks A and B, the typical appearance of sackungen on land is somewhat different because normally an uphill-facing scarp is the principal indication of the structure. In addition, the developing upslope gap or head scarp is commonly infilled to some extent by slope wash and other processes. In the marine examples of the present study, a deep and vertical head scarp remains. The sackung style of slope and bedrock deformation has not been observed in other British Columbia fjords examined to date (Conway et al. 2013), and these examples are the first to be identified from a submarine setting. In addition to vertically down relative motion, some lateral downslope movement of the sackungen blocks A and B is apparent. The kinematics and mechanisms of sackungen development represent a continuum with some elements of early stage landsliding involved in some described sackungen (Hutchinson 1988).

Conclusions

The Douglas Channel sackungen were emplaced very shortly after deglaciation over a period of several hundred to possibly as long as 2,400 years between approximately 15,800 and 13,400 calendar years ago. They have been inactive or only slowly moving during the last 11,000 years and are among the most precisely dated sackungen globally. Faults detected in the sub-bottom seismic data and onshore in topographic datasets are evidence of bedrock structural control of the form

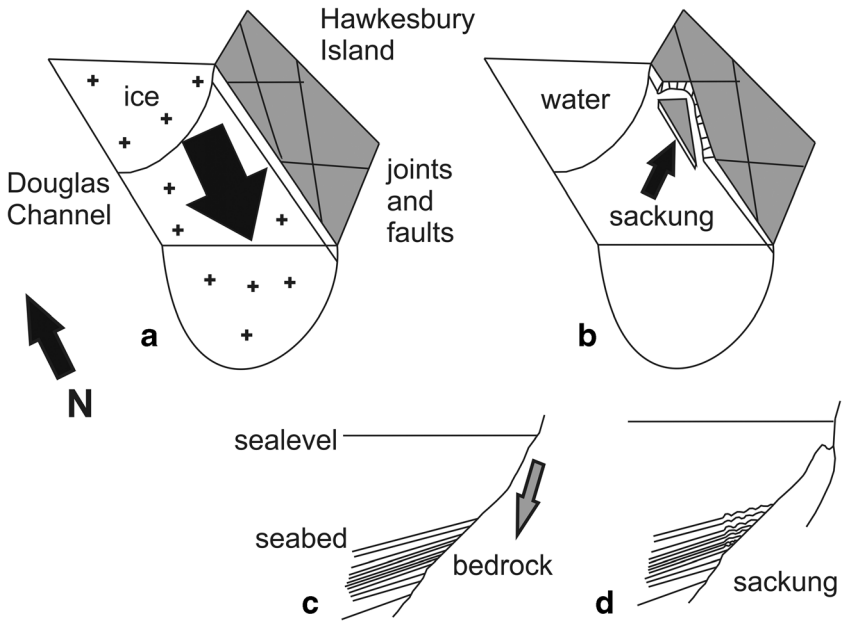

Fig. 12 Illustration of submarine sackung development in Douglas Channel. **a** Before sackung formation during glaciation. **b** Formation of sackung controlled by faults and joints following deglaciation. **c** Bedrock and sediment on fjord wall before sackung formation. **d** Bedrock and sediment deformation after sackung formation

and scale of the bedrock failures. Numerous small landslides associated with the submarine sackungen suggest ongoing slope instability may still exist. Detailed analysis of LiDAR and structural geology data is underway to examine the regional context in which the sackungen occur.

Acknowledgements Gwyn Lintern provided vital support as project leader, and at sea support by Greg Middleton and Peter Neelands is gratefully acknowledged. John Shaw provided insightful discussions. Thanks to Burg Fleming for a very helpful review that improved the paper.

Compliance with ethical standards

Conflict of interest The authors declare that there is no conflict of interest with third parties.

References

Agliardi F, Crosta GB, Zanchi A (2001) Structural constraints on deep-seated slope deformation kinematics. Eng Geol 59(1-2):83–102. https://doi.org/10.1016/S0013-7952(00)00066-1

Ambrosi C, Crosta GB (2005) Large sackung along major tectonic features in the central Italian alps. Eng Geol 83:183–200

Bianchi Fasani G, Di Luzio E, Esposito C, Evans SG, Scarascia Mugnozza G (2014) Quaternary catastrophic rock avalanches in the central Apennines (Italy): relationships with inherited tectonic features, gravity-driven deformations and the geodynamic frame. Geomorphology 211:22–42. https://doi.org/10.1016/j.geomorph.2013.12.027

Blais-Stevens A, Claque JJ, Mathewes RW, Hebda RJ, Bornhold BD (2003) Record of large, late Pleistocene outburst floods preserved in Saanich inlet sediments, Vancouver Island, Canada. Quat Sci Rev 22(21-22):2327–2334. https://doi.org/10.1016/S0277-3791(03)00212-9

Bornhold BD (1983) Sedimentation in Douglas Channel and Kitimat arm. Canadian Hydrography and Ocean Sciences Technical Reports 18:1–218

Bornhold BD, Thomson RE (2012) Tsunami hazard assessment related to slope failures in coastal waters. In: Clague JJ, Stead D (eds) Landslides – types, mechanisms and modeling, Cambridge University press, Cambridge, chapter, vol 10, pp 108–120. https://doi.org/10.1017/CBO9780511740367.011

Bornhold BD, Harper JR, McLaren D, Thomson RE (2007) Destruction of the first nations village of Kwalate by a rock avalanche-generated tsunami. Atmosphere-Ocean 45(2):123–128. https://doi.org/10.3137/ao.450205

Boyles JM, Scott AJ, Rine JM (1986) A logging form for graphic descriptions of core and outcrop. J Sediment Petrol 56(4):567–568. https://doi.org/10.1306/212F89DB-2B24-11D7-8648000102C1865D

Brückl EP (2001) Cause-effect models of large landslides. Nat Hazards 23(2/3):291–314. https://doi.org/10.1023/A:1011160810423

Clague JJ (1984) Quaternary geology and geomorphology of the Smithers-terrace-Prince Rupert area, British Columbia. Geological survey of Canada Memoir 413, 82 pp

Clague JJ (1985) Deglaciation of the Prince Rupert - Kitimat area, British Columbia. Can J Earth Sci 22(2):256–265. https://doi.org/10.1139/e85-022

Conway KW, Barrie JV (2015) Large submarine slope failures and associated Quaternary faults in Douglas Channel, British Columbia. Geological Survey of Canada, Current Research 2015-9, 12 pp. doi:https://doi.org/10.4095/297316

Conway KW, Barrie JV, Hebda RJ (2001) Evidence for a late quaternary outburst flood event in the Georgia Basin, British Columbia. Geological Survey of Canada, Current Research 2001-A13, 6 pp

Conway KW, Barrie JV, Thomson RE (2012) Submarine slope failures and tsunami hazard in coastal British Columbia: Douglas Channel and Kitimat Arm. Geological Survey of Canada, Current Research 2012-2010, 13 pp. doi:https://doi.org/10.4095/291732

Conway KW, Kung RB, Barrie JV, Hill PR, Lintern DG (2013) A preliminary assessment of the occurrence of submarine slope failures in Coastal British Columbia by analysis of swath multibeam bathymetric data collected 2001b-2011. Geol Surv Canada, Open File 7348. https://doi.org/10.4095/292370

Crosta C, Frattini P, Agliardi F (2013) Deep seated gravitational slope deformations in the European Alps. Tectonophysics 605:13–33. https://doi.org/10.1016/j.tecto.2013.04.028

Duffell S, Souther JG (1964) Geology of the terrace map area, British Columbia (103 1E). Geol Surv Canada Memoir 329, 117 pp

Fairbanks RG, Mortlock RA, Chiu T, Cao L, Kaplan A, Guilderson TP, Fairbanks TW, Bloom AL (2005) Marine radiocarbon calibration curve spanning 0 to 50,000 years B.P. based on paired $^{230}Th/^{234}U/^{238}U$ and ^{14}C dates on pristine corals. Quat Sci Rev 24(16-17):1781–1796. https://doi.org/10.1016/j.quascirev.2005.04.007

Forcella F (1984) The Sackung between mount Padrio and mount Varadega, central alps, Italy: a remarkable example of slope gravitational tectonics. Méditerranée, Troisième série 51(1-2):81–92. https://doi.org/10.3406/medit.1984.2237

Gutiérrez F, Acosta E, Ríos S, Guerrero J, Lucha P (2005) Geomorphology and geochronology of sackung features (uphill-facing scarps) in the central Spanish Pyrenees. Geomorphology 69(1-4):298–314. https://doi.org/10.1016/j.geomorph.2005.01.012

Helm A (1932) Bergsturz und Menschenleben. Fretz und Wassermuth, Zürich, Switzerland, 218 pp

Hetherington R, Barrie JV, Reid RGB, MacLeod R, Smith DJ (2004) Paleogeography, glacially induced crustal displacement, and late quaternary coastlines on the continental shelf of British Columbia Canada. Quat Sci Rev 23(3-4):295–318. https://doi.org/10.1016/j.quascirev.2003.04.001

Hewitt K, Clague JJ, Orwin JF (2008) Legacies of catastrophic rock slope failures in mountain landscapes. Earth Sci Rev 87(1-2):1–38. https://doi.org/10.1016/j.earscirev.2007.10.002

Hippolyte JC, Bourlès D, Léanni L, Braucher R, Chauvet F, Lebatard AE (2012) ^{10}Be ages reveal >12 ka of gravitational movement in a major sackung of the Western Alps (France). Geomorphology 171-172:139–153. https://doi.org/10.1016/j.geomorph.2012.05.013

Holland S (1976) Landforms of British Columbia – a physiographic outline. British Columbia Department of Mines and Petroleum Resources, Bulletin 48, 138 pp

Hutchinson JN (1988) General report: morphological and geotechnical parameters of landslides in relation to geology and hydrogeology. In: Bonnard C (ed) Proc 5th Intl Symp landslides, Lausanne, Switzerland. Balkema, Rotterdam, pp 3–35

Johannessen SJ, Wright CA, Spear DJ (2015) Seasonality and physical control of water properties and sinking and suspended particles in Douglas Channel, British Columbia. Canadian hydrography and ocean sciences, technical reports 308, 26 pp

Li Z, Bruhn RL, Pavlis TL, Vorkink M, Zeng Z (2012) Origin of sackung uphill-facing scarps in the Saint Elias orogen, Alaska: LIDAR data visualization and stress modeling. GSA Bull 122(9-10):1585–1599. https://doi.org/10.1130/B30019.1

Macdonald RW, Bornhold BD, Webster I (1983) The Kitimat fjord system: an introduction. Canadian Hydrography and Ocean Sciences, Technical Reports 18:2–13

Mazzotti S, Hyndman RD, Flück P, Smith AJ, Schmidt M (2003) Distribution of the Pacific/North America motion in the Queen Charlotte Islands - S. Alaska plate boundary zone. Geophys Res Lett 30(14):1762. https://doi.org/10.1029/2003GL017586

Mazzotti S, Leonard LJ, Cassidy JF, Rogers GC, Halchuk S (2011) Seismic hazard in western Canada from GPS strain rates versus earthquake catalog. J Geophys Res 116(B12): B12310. https://doi.org/10.1029/2011JB008213

McCalpin JP, Hart EW (2002) Ridge top spreading features and relationship to earthquakes, San Gabriel Mountains, Southern California. Part B: Paleoseismic investigations of ridge-top depressions. U.S. Geological Survey, National Earthquake Hazards Reduction Program, Final Technical Report 99HQGR0042

Mosher DM (2009) Submarine landslides and consequent tsunamis in Canada. Geosci Can 36(4):179–219

Nelson JL, Diakow LJ, Mahoney JB, van Staal J, Pecha M, Angens JJ, Gehrels G, Lau T (2011) North coast project: tectonics and metallogeny of the Alexander terrane and cretaceous sinistral shearing of the western Coast Belt. BC Ministry of Energy and Mines, Geological Fieldwork Paper 2011. http://www.empr.gov.bc.ca

Pánek T, Mentlík P, Ditchburn B, Zondervan A, Norton K, Hradecký J (2015) Are sackungen diagnostic features of (de)glaciated mountains? Geomorphology 248:396–410. https://doi.org/10.1016/j.geomorph.2015.07.022

Poisel R, Preh A (2004) Rock slope initial failure mechanisms and their mechanical models. Felsbau 22:40–45

Poisel R, Preh A (2008) Landslide detachment mechanisms: an overview of their mechanical models. In: Ho K, Li V (eds) Proc 2007 Intl Forum Landslide Disaster Management, 10–12 December 2007, Hong Kong, pp 1043–1058

Roddick JA (1970) Douglas Channel-Hecate Strait map area, British Columbia (103 H). Geological Survey of Canada, Paper 70-41, 56 pp

Sanchez G, Rolland Y, Corsini M, Braucher R, Bourlès D, Arnold M, Aumaître G (2010) Relationships between tectonics, slope instability and climate change: cosmic ray exposure dating of active faults, landslides and glacial surfaces in the SW alps. Geomorphology 117(1-2):1–13. https://doi.org/10.1016/j.geomorph.2009.10.019

Schwab JW, Kirk M (2002) Sackungen on a forested slope, Kitnayakwa River, Prince Rupert Forest region. British Columbia Forest Service, extension note #47

Shaw J, Stacey CD, Wu Y, Lintern DG (2017) Anatomy of the Kitimat fiord system, British Columbia. Geomorphology 293:108–129. https://doi.org/10.1016/j.geomorph.2017.04.043

Soldati M (2013) Deep-seated gravitational slope deformation. In: Bobrowsky PT (ed) Encyclopedia of natural hazards. Springer, Dordrecht, pp 151–154. https://doi.org/10.1007/978-1-4020-4399-4_86

St. Onge G, Mulder T, Piper DJW, Hillaire-Marcel M (2004) Earthquake and flood induced turbidites in the Saguenay Fjord (Quebec): a Holocene paleoseismicity record. Sci Rev 23(3-4):283–294. https://doi.org/10.1016/j.quascirev.2003.03.001

Thompson SC, Clague JJ, Evans SG (1997) Holocene activity of the Mt. Currie scarp, Coast Mountains, British Columbia, and implications for its origin. Eng Geosci III(3):329–348. https://doi.org/10.2113/gseegeosci.III.3.329

Thomson RE, Fine I, Krassovski M, Cherniawsky J, Conway KW, Wills P (2012) Numerical simulation of tsunamis generated by submarine slope failures in Douglas Channel, British Columbia. Department of Fisheries and Oceans, Canadian science advisory research document 2012/115, 38 pp

Weiss R, Fritz JM, Wünnemann K (2009) Hybrid modeling of the mega-tsunami runup in Lituya Bay after half a century. Geophys Res Lett 36(9):L09602. https://doi.org/10.1029/2009GL037814

Wentworth CK (1923) A scale of grade and class terms for clastic sediments. J Geol 30:377–392

Wheeler JO, Brookfield AJ, Gabrielse H, Monger JWH, Woodsworth GJ (1991) Terrane map of the Canadian Cordillera. Geological Survey of Canada, Map 1713A, scale 1:2 000 000

Zischinsky U (1966) On the deformation of high slopes. In: ISRM Proc 1st Conf International Society for Rock Mechanics, 25 Sept.–1 Oct. 1966, Lisbon, Section 2, pp 179–185